Race Motorcycle Smart Wheel

Massimiliano Gobbi, Giampiero Mastinu, Federico Ballo, and Giorgio Previati
Politecnico di Milano

CONTACT INFORMATION

Prof. Massimiliano Gobbi
massimiliano.gobbi@polimi.it
tel.: +39 02 2399 8214

INTRODUCTION

The knowledge of the force acting at the tyre-road interface is of crucial importance for the optimal setup of race motorcycles.

In case of motorcycles, there is a very wide variety of driving situations, load conditions and driving styles to be considered. Numerical simulations can provide a rough idea of the possible maximum loads on the wheels but a large amount of uncertainty still remains [1].

In this paper, the real time measurement of the force at the tyre-road interface by an innovative measuring wheel is considered. The wheel [2, 3, 4, 5, 6] able to measure the forces and moments at tyre-road interface is designed to be fitted at the front of a race motorcycle to be used to measure the forces while driving on a race track. An accurate knowledge of the force transmitted by the tyres will allow the designers to optimize the suspension settings and to improve the design of the wheel itself.

The measure of the forces and moments at the interface between the tire and road has been widely discussed in the literature and many applications can be found referring to devices developed for such measurements ([7,8]). The sensing unit of such measuring systems can be realized by means of strain gauges ([9,10,12]) or piezo-resistive sensors [11]. Different measuring hubs are present on the market [1,2,3,4,5,6], [9,10,11,12]). Most of them are characterized by complex hardware and the ones developed for motorcycles [9] are difficult to apply to race motorcycles due to their excessive mass.

This paper is focused on the development of a new measuring wheel, similar to the ones presented in [2,25]. The design of this smart wheel has been realized on the basis of the patented [14,15] system described in [16,17]. The resulting measuring wheel is ideally a statically determined three spoke structure connecting the hub to the rim of the wheel. The three spoke structure is connected to the rim by means of specially designed (and patented) sliding spherical joints ([18,19]). The stiffness of the joints make the structure quasi-statically determined. The deformation of the three spoke structure is measured by means of strain gauges and related to the actual forces and moments acting between the tire and the road.

The first section of the paper describes the models (analytical and FE) used during the development of motorcycle measuring wheel. The mechanical design is presented in the second section of the paper. The electronic hardware is described in section 4. Finally the calibration of the sensor and the some experimental test data are reported.

MEASURING WHEEL MODELLING

The concept design of the developed smart wheel for measuring forces and moments is shown in Fig. 1 ([2,3,4,5,6], [16,17], [25]).

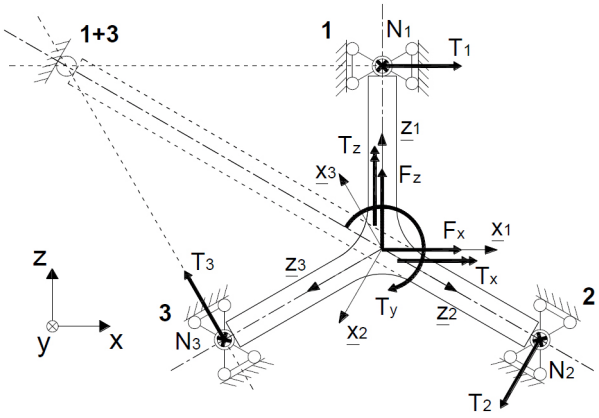

Fig. 1. Concept design of the smart wheel.

The three spoke structure is constrained to the rim by means of three joints positioned at the tip of each spoke. The joints are plates located between each spoke tip and the rim (see Fig. 2). Their shape has been optimized in order to reproduce a joint with very low axial and rotational stiffness. The final aim is to obtain a quasi-statically determined structure by constraining the tip of each spoke to the rim by means of translating spherical joints (1, 2, 3 in Fig. 1). Fig. 1 shows that the two constraints at two adjacent cantilevers/spokes (e.g. 1, 3) are equivalent to the virtual rotational joint (1+3).

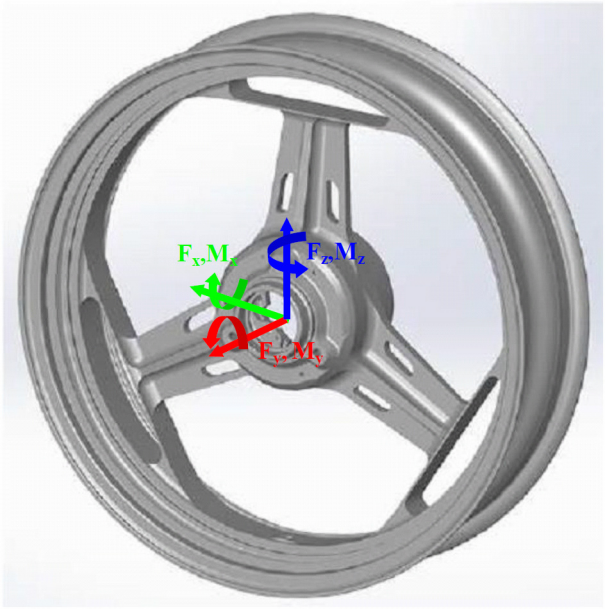

Figure 2. Measuring wheel structural model. The global coordinate system is highlighted.

With this type of structure, each spoke tip is subject to two forces only, so that a total of 6 forces are acting at the three spoke tips. Namely, there are the three forces T_1 T_2 T_3 and other three forces N_1 N_2 N_3 normal to them. The six forces T_i, N_i at the spoke tips can be measured by sensing the strain level due to the bending moments at each spoke root. Given such six forces, the three forces and the three moments at the centre of the sensor **F** can be computed by solving simple equilibrium equations.

The solid model of the smart wheel is shown in Fig.2.

The three cantilever/spoke structures are instrumented by means of 12 strain gauges at the positions shown in Fig. 3 and connected in half-bridge configuration. Their positions have been defined in order to maximize the output (voltage) of the strain gauges for all combinations of loads applied at the wheel centre. The strain gauges resistance is 350 Ω, sufficiently high to limit the wheel power requirement.

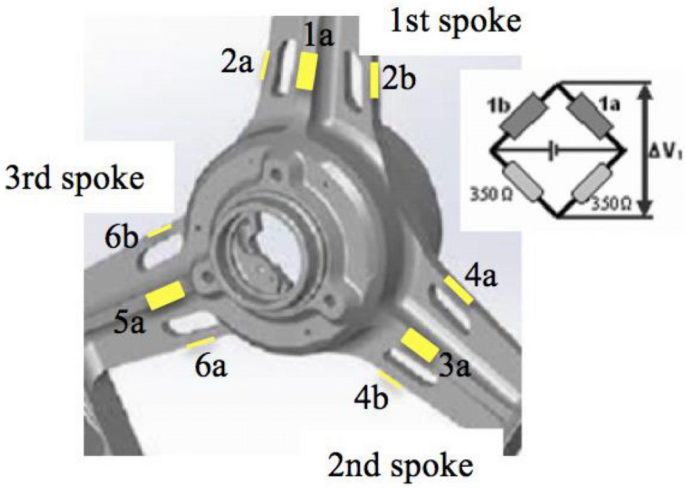

Figure 3. Location of the 12 strain gauges.

The strain gauges are intentionally located in the area where the bending moments acting at each cantilever/spoke produce high strains.

The theoretical calibration matrix has been derived to compute the vector of the forces and moments acting on the sensor given the strain gauge measures.

On the basis of the simple model which considers the smart wheel as a statically determined structure (Fig. 1), a more refined analytical model describing the wheel as a quasi-statically determined structure, (i.e. statically undetermined structure) has been derived taking into account the compliance of the elastic sliding spherical joints (see [16]).

A set of six stiffness has been introduced in order to model each joint at the spoke tip (axial 'k_a', radial 'k_{rx} - k_{ry}', torsional 'k_t' and bending 'k_{bt} - k_b' stiffness) and a central rigid ring has been considered for taking into account the very stiff central part of the smart wheel (Fig. 4).

A central rigid ring has been included to model the wheel hub. The structure with the central rigid ring can be considered equivalent to a structure in which the three spokes are connected at the centre and each spoke is divided into two parts. The first part of the spoke, from the tip to the connection with the rigid ring, is considered as a deformable beam. The second part of the spoke, from the centre of the structure to the external part of the rigid ring, is considered as a rigid beam, see Fig. 5. The spokes have been modelled as tapered beams.

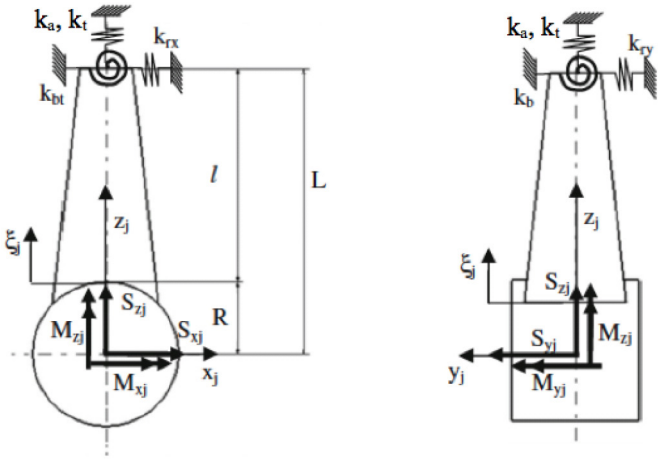

Figure 4. Single spoke representation of the statically undetermined structure with a central rigid ring.

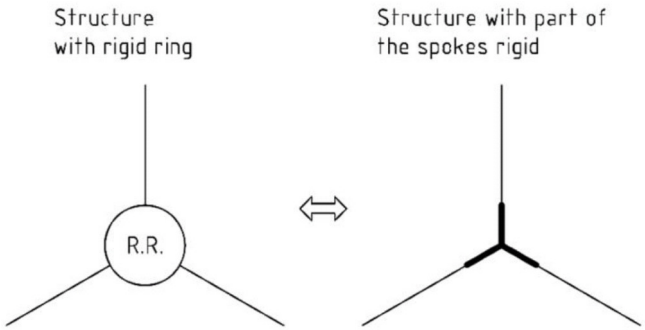

Figure 5. Wheel structure with a central rigid ring. Bold line: rigid partitions of the spokes.

The analytical expressions of the equations system which allows to estimate the output differential voltages *AVj* at the Wheatstone bridges as a function of the system parameters (joint stiffness, three spoke structure geometry, strain gauges characteristic,…) and of the vector **F** of the forces and of the moments acting at the smart wheel are reported in [16]. A discussion on the theoretical performances and error propagation of this type of sensors is reported in [17].

By defining the vector of the forces and of the moments acting at the centre of the wheel (see the coordinate system in Fig. 1) as

$$\mathbf{F} = \left[F_x \; F_y \; F_z \; T_x \; T_y \; T_z\right]^T$$

and the vector of the strains measured at the locations shown in Fig. 2

$$\mathbf{E_S} = \left[\varepsilon_{1a} \; \varepsilon_{1b} \; \varepsilon_{2a} \; \varepsilon_{2b} \; \varepsilon_{3a} \; \varepsilon_{3b} \; \varepsilon_{4a} \; \varepsilon_{4b} \; \varepsilon_{5a} \; \varepsilon_{5b} \; \varepsilon_{6a} \; \varepsilon_{6b}\right]^T$$

The following relationship holds

$$\mathbf{F} = \mathbf{F}\left(\mathbf{E_S}\right) \tag{1}$$

The above equation becomes

$$\mathbf{F} = \mathbf{C} \cdot \mathbf{E_S} \tag{2}$$

if a linear relationship between **F** and $\mathbf{E_S}$ holds.

A suitable connection (half bridge) of the strain gauges allows the measurement of two bending moments. Therefore the vector of the bending strains signals reduces to $\mathbf{E_b}=[\varepsilon_1 \; \varepsilon_2 \; \varepsilon_3 \; \varepsilon_4 \; \varepsilon_5 \; \varepsilon_6]^T$.

The relationship between **F** and $\mathbf{E_b}$ becomes

$$\mathbf{F} = \mathbf{C_b} \cdot \mathbf{E_b} \tag{3}$$

where $\mathbf{C_b}$ is a 6×6 constant square matrix referred as sensor calibration matrix.

The relationship between the vector of the bridges output voltages **ΔV** and the vector **F** is the theoretical calibration matrix $\mathbf{M_{tst}}$

$$\mathbf{F} = \mathbf{M_{tst}} \cdot \mathbf{\Delta V} \tag{4}$$

MECHANICAL DESIGN

The measuring wheel has to be designed in order to have mass and stiffness properties similar to those of the standard racing wheel while providing a good sensitivity [6].

The design of the measuring wheel has been performed in three stages

1. Preliminary design, definition of the geometrical dimensions of the spokes and of the joint stiffness by means of the analytical model previously described
2. Joints design, design of the connecting plates in order to get the desired joint stiffness by using a finite element code
3. Detail design of the full wheel

In the first phase the most important parameters of the measuring wheel (material, spoke length, cross section and tapering) are selected in order to meet the prescribed values of mass and stiffness and to obtain a high level of deformation at the strain gauges locations.

A magnesium alloy with a good combination of mechanical properties and corrosion resistance has been selected.

Additionally, target values for the stiffness of the joint have been set in order to have a structure close to a statically determined one (i.e. axial and rotational joints stiffness have to be small with respect to the radial joint stiffness). In fact, as explained in [17,25], the strain level read by the strain gauges drop if the structure becomes statically undetermined, i.e. axial and rotational stiffness of the joints are above a critical value depending on the geometry of the measuring wheel.

A multi-objective optimization approach has been applied [20,22,27] in the first design stage. The system has been optimised by considering two loading conditions. For both manoeuvres, a static

load of 2 kN has been considered in the vertical direction. To account for bumps and other dynamic loads, this value has been multiplied by 2.5. So, a maximum vertical force of 5 kN has been applied to the measuring wheel. During the brake manoeuver, a longitudinal force of 3 kN has been added, while during the turning manoeuver a lateral force of 1.5 kN has been included.

The design variables are the spoke cross section dimensions a and b (Fig. 6), the spoke length and tapering and the joint stiffness (axial k_a, radial k_{rx}-k_{ry} and bending k_b-k_{bt}). The spoke cross section has been chosen in order to have a low torsional stiffness. In fact, the connecting plate between each spoke and the wheel rim can be designed to have very low bending stiffness, but the torsional compliance must be allowed by designing deformable spokes (i.e. the torsional stiffness k_t is not a design variable but depends on the spoke geometry, see *a* and *b*, in Fig. 6).

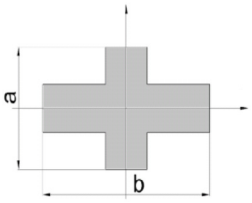

Figure 6. Spoke cross section.

The inertia properties (torsional and bending) of the selected section is given in analytical form in [26]. The spoke length is actually set to the maximum allowable value since the sensor sensitivity is proportional to this value (see [17]).

The optimal design problem is defined as follows

- mass as close as possible to a target mass value
- radial stiffness of the measuring wheel as close as possible to a target value
- high strain levels at strain gauges locations

under the obvious constraint that the wheel should survive the considered load cases. These objective functions and constraints can be translated into mathematical form as functions of the design variables by applying the analytical model previously described (see section 1). The result is a vector of objective functions which has to be minimized by solving a multiobjective optimization problem [22]. By this approach the final solution is found as the best compromise between the three different objective functions [20].

In the second design phase, the geometry of the connecting plate between the spoke and the wheel rim is optimally designed in order to reproduce the axial, radial and torsional stiffness defined in the previous phase. A FE model (Fig.7) of the plate is realized in order to compute the stiffness of the joint and to verify its mechanical resistance for the considered load cases.

In the final design stage, the full FE model of the wheel is developed (see Fig. 8). The full FE model of the measuring wheel (Fig.8) is used to verify the wheel performance (mass, stiffness, sensitivities). The wheel is fixed on the outer rim as shown in Fig. 8. Vertical, lateral and longitudinal loads are applied at the wheel centre, rigidly connected to the two bearing housings. Second order tetraedrical elements have been employed for meshing the component..

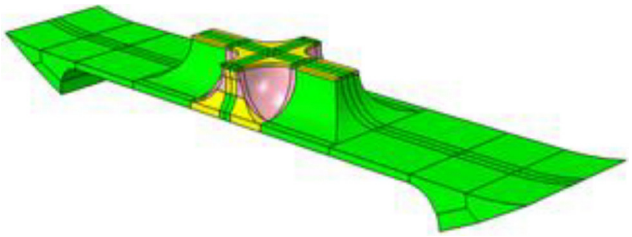

Figure 7. FE model of the elastic joint between the spoke and the rim.

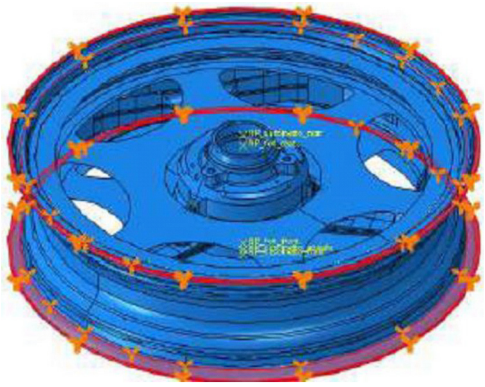

Figure 8. FE model of the measuring wheel.

This FE model has shown a dependence of the sensor sensitivity and of the radial stiffness on the angular position of the wheel i.e. the reading of the strain gauges depend on the angular position of the wheel at a constant loading condition.

Four magnesium disks (two for each rim side, see Fig. 8 and 9) have been added to limit this effect in order to make the radial stiffness quite uniform.

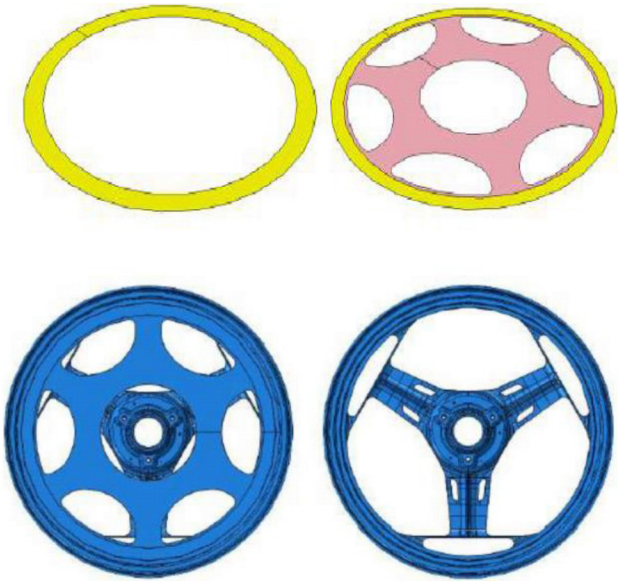

Figure 9. Stiffening disks (outer disk on left side and inner disk on right side). The final layout of the wheel with stiffening disks is shown on the bottom.

The annular disk geometry is shown in Fig. 9. Large size holes are present to limit the aerodynamic effect of the wheel at high speed. The magnesium disks are press fitted and glued to the rim in order to increase the radial stiffness uniformity of the rim without connecting the rim with the hub.

A relevant improvement in radial stiffness uniformity is shown in Tab. 1.

Table 1. Variation of the radial stiffness with respect to the wheel angular position. Only minimum and maximum stiffness are reported.

	Radial stiffness MIN [N/m]	Radial stiffness MAX [N/m]
With no stiffening disks	3E6	8E6
With stiffening magnesium disks	9E6	10E6

The structural integrity of the measuring wheel has been checked by considering the static load cases previously described and the fatigue life of the wheel. The fatigue life of the wheel has been computed by considering standard load spectra used by the wheel manufacturer. The considered vertical force, bending moment and torsional moment load spectra have been derived on the basis of the manufacturer experience.

The new measuring wheel itself is currently used to obtain more accurate load spectra.

The Palmgren-Miner rule [23] has been applied to estimate the fatigue life of the wheel. This rule is based on the Wöhler diagram for the material and it estimates the fraction of damage d_i of a mechanical component subject to n_i cycles at a stress condition σ_i^*, as $d_i = n_i / N_i$, where N_i is the maximum number of cycles that the component can withstand at the stress level σ_i^* (see Fig.10).

The Palmgren-Miner rule states that failure will not occur if the sum of the damages d_i is less than 1.

The Wöhler diagram is derived from tests on specimens by applying a sinusoidal bending stress. In case of multi-axial stress, a scalar reference stress must be derived from the multi-axial stress condition [24]. In this work, the reference stress σ_i^* described in eq. 5 by Sines [24] has been used. This reference stress takes into account both the external forces that give constant stresses on the wheel (for instance the axial torque My) and the forces that cause alternate stresses (for instance the vertical load Fz).

$$\sigma_i^* = \frac{\sqrt{\sigma_{Ia}^2 + \sigma_{IIa}^2 + \sigma_{IIIa}^2 - \sigma_{Ia}\sigma_{IIa} - \sigma_{Ia}\sigma_{IIIa} - \sigma_{IIa}\sigma_{IIIa}}}{1 - \frac{I_m}{R_m}} \quad (5)$$

with

$$I_m = \frac{\sigma_{Im} + \sigma_{IIm} + \sigma_{IIIm}}{3}$$

where

$\sigma_{Im}, \sigma_{IIm}, \sigma_{IIIm}$ principal constant stresses

$\sigma_{Ia}, \sigma_{IIa}, \sigma_{IIIm}$ principal alternate stresses

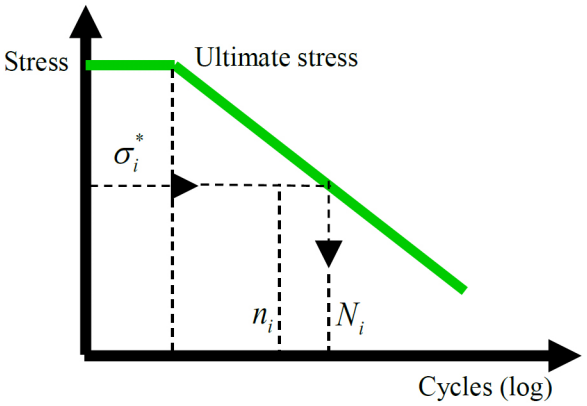

Figure 10. Simplified Wöhler diagram for a magnesium alloy.

DATA ACQUISITION SYSTEM DESIGN

As the measuring hub rotates, a telemetry system has been especially designed and developed to transmit the six voltage signals from the strain gauges to a storage system on board of the vehicle.

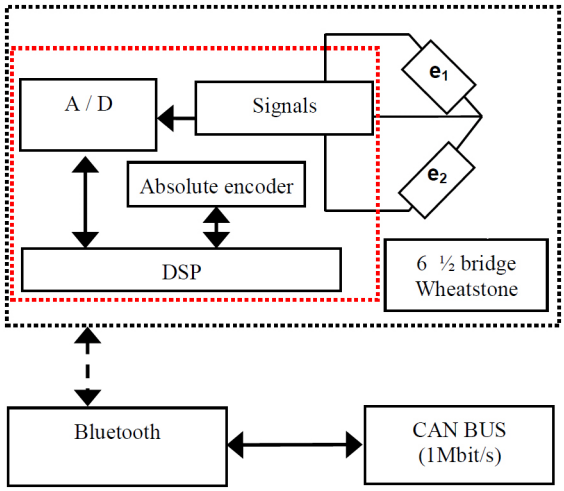

Figure 11. Hardware block diagram.

Utilizing an encoder (angular resolution 0.05°), a simultaneous ADC (Analog to Digital Converter) sampling is performed on the six strain gauges bridges outputs while coupling the force/torque output with the absolute wheel angular position. The synchronous sampling allows seamless real-time measurements at vehicle speed up to 400 km/h.

The real-time calculation of the forces/torques components is performed by a DSP programmed to apply the calibration matrix and the rotation matrix.

The signals are sent via Bluetooth to an onboard receiver connected to the vehicle CAN bus. Each signal is sampled at 200Hz. The wheel can be used to derive the tyre characteristics or just to record the actual loads acting at the hub.

Fig. 11 shows the simplified block diagram of the acquisition data system.

CALIBRATION

A special calibration system has been designed and constructed for the calibration of the measuring wheel. It can apply different load combinations to the sensor in the vertical (Fz), longitudinal (Fx) and lateral (Fy) direction. The device is shown in Fig.12. By means of this system, a large number of different load combinations can be applied to the measuring wheel. The definition of the calibration matrix M_e is based on a least squares method.

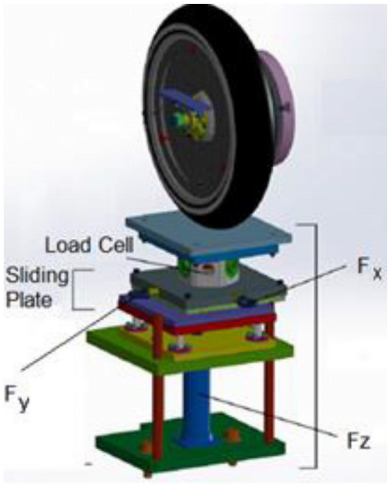

Figure 12. Calibration system.

Let us consider a load case denoted by the subscript k. By measuring the force applied by the calibration device, from the geometry of the fixture, the applied load vector $\mathbf{F_k}$ is known. The output of the six Wheatstone bridges is measured and recorded in $\Delta\mathbf{V_k}$. Then, for each applied load combination, by applying eq. 4, an error vector $\mathbf{e_k}$ can be defined

$$\mathbf{e_k} = \mathbf{F_k} - \mathbf{M_e} \cdot \Delta\mathbf{V_k} \tag{6}$$

If at least 6 linearly independent load cases are considered, the following calibration error can be defined

$$\mathbf{e}_{cal} = \mathbf{F}_{cal} - \mathbf{M_e} \cdot \Delta\mathbf{V}_{cal} \tag{7}$$

where

$$\mathbf{e}_{cal} = \begin{bmatrix} \mathbf{e_1} & \mathbf{e_2} & \cdots & \mathbf{e_n} \end{bmatrix}, \quad \mathbf{F}_{cal} = \begin{bmatrix} \mathbf{F_1} & \mathbf{F_2} & \cdots & \mathbf{F_n} \end{bmatrix},$$
$$\Delta\mathbf{V}_{cal} = \begin{bmatrix} \Delta\mathbf{V_1} & \Delta\mathbf{V_2} & \cdots & \Delta\mathbf{V_n} \end{bmatrix}$$

being n the number of tests. And the squared error is

$$\mathbf{E} = \mathbf{e}_{cal} \cdot \mathbf{e}_{cal}^T \tag{8}$$

By minimizing the squared error, the following relationship can be derived

$$\frac{\partial \mathbf{E}}{\partial \mathbf{M_e}} = \mathbf{0} \Rightarrow 2\Delta\mathbf{V}_{cal}\left(\Delta\mathbf{V}_{cal}^T \cdot \mathbf{M_e}^T - \mathbf{F}_{cal}^T\right) = \mathbf{0} \tag{9}$$

And finally the calibration matrix is obtained from eq. 9 by computing the pseudo-inverse of $\Delta\mathbf{V}$

$$\mathbf{M_e}^T = inv(\Delta\mathbf{V}_{cal} \cdot \Delta\mathbf{V}_{cal}^T) \cdot \Delta\mathbf{V}_{cal} \cdot \mathbf{F}_{cal}^T \tag{10}$$

The prototype measuring wheel shown in Fig. 8, has been calibrated by applying a very large number of load combinations.

The results of the calibration process are described in the following plots.

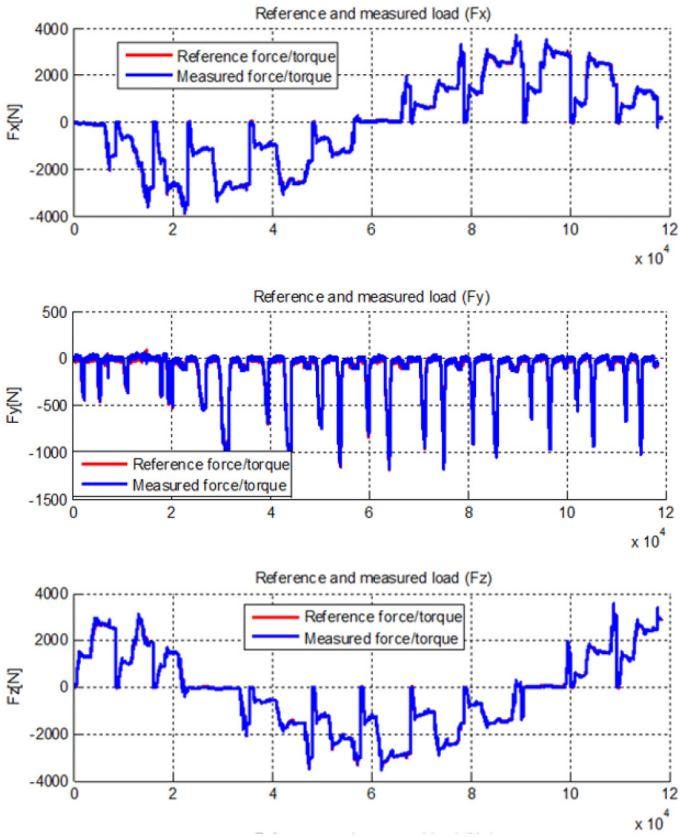

Figure 13. Reference and measured forces after sensor calibration.

Fig. 13 and 14 show the comparison between the reference loads and the measuring wheel outputs. The accuracy of the sensor is very good in the whole measuring range.

The cross talk is lower than 2% of the full scale.

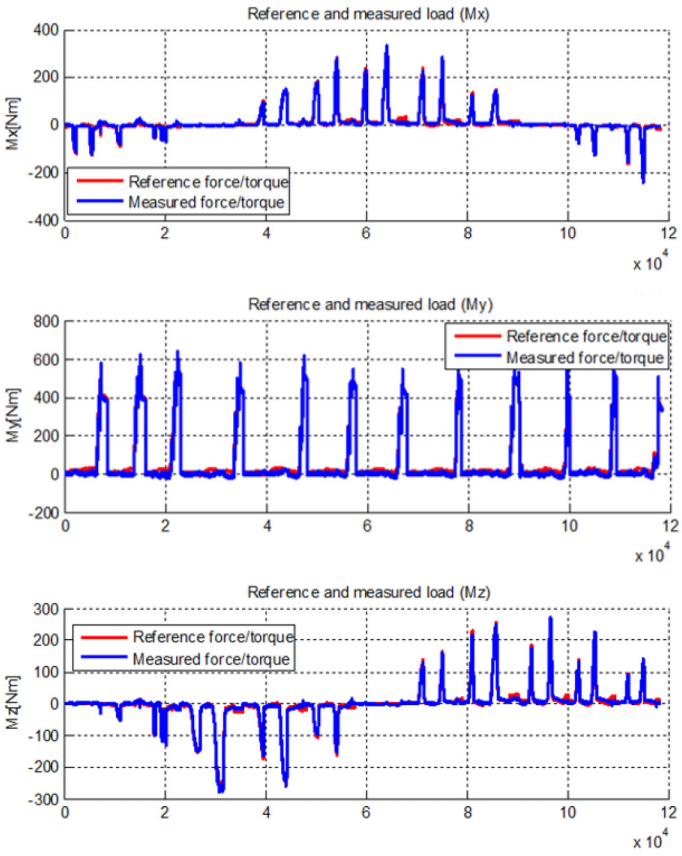

Figure 14. Reference and measured moments after sensor calibration.

The measurement error distribution is Gaussian, with a standard deviation significantly below 1% of the full scale for both forces and torques. An example is shown in Fig. 15.

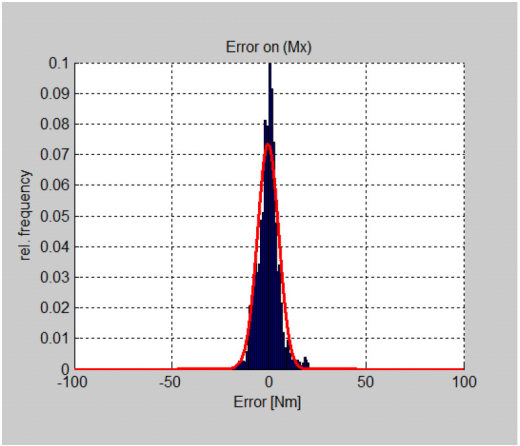

Figure 15. Error distribution for Mx.

The linearity of the sensor is very good as shown in Fig. 16.

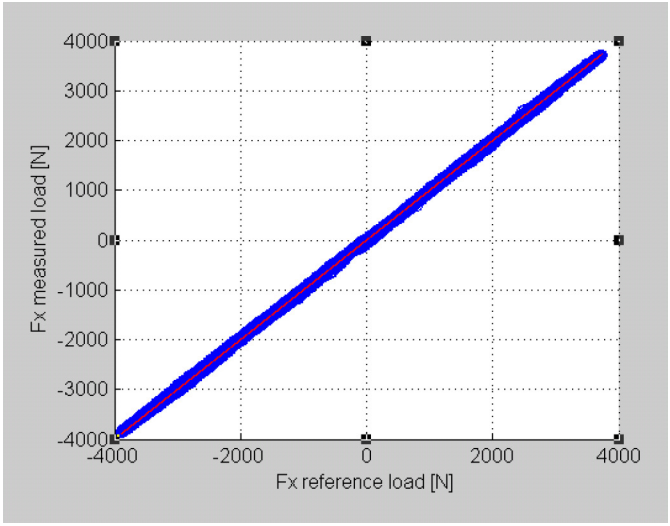

Figure 16. Linearity plot for Fx.

The coefficient of determination (R^2) of the linear regression between actual and measured forces/torques is always close to 1, see Tab. 2 for details.

Table 2. R^2 values for the three forces and moments show the linear behaviour of the measuring wheel. A linearity plot is shown in Fig. 16.

Force/Moment	R^2
Fx	1
Fy	0.997
Fz	1
Mx	0.994
My	0.998
Mz	0.996

The experimentally derived calibration matrix (see eq. 10) M_e reads

$$M_e = \begin{bmatrix} 0.025 & 0.510 & -0.003 & -0.251 & 0.000 & -0.268 \\ 0.199 & -0.014 & 0.202 & -0.015 & 0.200 & -0.013 \\ -0.003 & 0.011 & 0.006 & -0.456 & 0.006 & 0.442 \\ -0.031 & 0.000 & 0.015 & 0.001 & 0.015 & 0.001 \\ -0.003 & 0.073 & -0.007 & 0.075 & -0.005 & 0.073 \\ 0.000 & 0.001 & 0.028 & -0.001 & -0.026 & -0.000 \end{bmatrix}$$

which is consistent, for the relevant terms, with the one derived by the analytical model described in Section 1 (Measuring Wheel Modelling).

$$M_{tst} = \begin{bmatrix} 0 & 0.490 & 0 & -0.246 & 0 & -0.246 \\ 0.231 & 0 & 0.231 & 0 & 0.231 & 0 \\ 0 & 0 & 0 & -0.425 & 0 & 0.425 \\ -0.047 & 0 & 0.023 & 0 & 0.023 & 0 \\ 0 & 0.080 & 0 & 0.080 & 0 & 0.080 \\ 0 & 0 & 0.039 & 0 & -0.039 & 0 \end{bmatrix}$$

TESTING

High speed tests have been performed on the Ruotavia test rig [5]. The experimental setup is shown in Fig. 17. The measuring wheel has been installed on a motorcycle suspension system.

Figure 17. High speed indoor testing (up to 310 km/h) on the ruotavia test rig.

The measured forces/moments are reported in Fig. 18. The increase in vertical loading is due to the dynamic deformation of the tyre under centrifugal forces.

Track tests have confirmed the accuracy and reliability of the measuring wheel in actual running conditions.

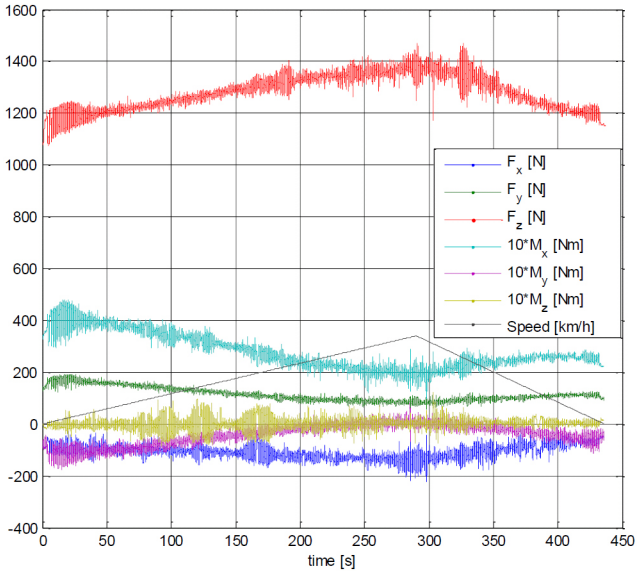

Figure 18. Data acquisition during high speed testing.

CONCLUSIONS

In the paper, the design and calibration of a measuring wheel able to measure the generalized forces at the hub of a race motorcycle has been designed and tested.

The wheel has a very limited mass (about 2 kg). It is made from magnesium with a special structure to sense the forces and provide the required level of stiffness. The wheel has been tested both indoor for preliminary approval and on the track according to internal standards.

The procedure for the optimal design of the measuring wheel has been presented and discussed in the paper.

An analytical model of the measuring wheel has been derived and used to optimize the main parameters of the wheel in an early design stage. Particular attention has been devoted to the design of the joints connecting the sensing elements of the measuring hub to the wheel rim in order to achieve the correct stiffness of the joints. Then, a detailed FE model of the system has been used for the definition of the final geometry of the measurement wheel and to assess its fatigue life.

Stiffening magnesium disks have been introduced to obtain the required level of stiffness and measurement accuracy.

Utilizing an encoder, a simultaneous ADC sampling is performed on the six strain gauges bridges outputs while coupling the force/torque output with the absolute wheel angular position. The synchronous sampling allows seamless real-time measurements at vehicle speed up to 400 km/h. The signals are sent via Bluetooth to an onboard receiver connected to the vehicle CAN bus. Each signal is sampled at 200Hz.

The results of the experimental calibration of the measuring wheel have been analysed. The measurement error distribution is Gaussian, with a standard deviation significantly below 1% for both forces and moments. The accuracy of the sensor is very good in the whole measuring range with a cross-talk lower than 2%. The three forces and the three moments at the hub can be measured with a resolution of respectively 1N and 0.3Nm.

The wheel can be used to derive the motorcycle tyre characteristic or just to record the loads acting at the hub. An accurate knowledge of the force transmitted by the tyres will allow the designers to optimize the suspension settings and to improve the design of the wheel itself.

REFERENCES

1. Slimi H., Arioui H. and Mammar S. “Motorcycle Lateral Dynamic Estimation and Lateral Tire-Road Forces Reconstruction Using Sliding Mode Observer”, IEEE Intelligent Transportation Systems Conference (ITSC 2013), The Hague : Pays-Bas, 2013.
2. Gobbi M., Mastinu G., “Wheels with Integrated Sensors for Measuring Tyre Forces and Moments”, AVEC Conference, 2004.
3. Gobbi M., Mastinu G., Rocca G., “Design of a Smart Wheel”, (IDETC2008-49838). Proceedings of the 2008 International Design Engineering Technical Conference IDETC 2008, Information In Engineering Conference IDETC/CIE 2008, August 3-6, 2008, Brooklyn, New York, Usa, Isbn 0-7918-3831-5, 2008.

4. Gobbi M., Mastinu G., Rocca G., “A smart wheel for improving the active safety of road vehicles”, (IDETC2010-29059). Proceedings of the 2010 International Design Engineering Technical Conference IDETC 2010, August 15-18, 2010, Montreal, Canada.
5. Gobbi M., Mastinu G. and Giorgetta F., “Sensors for measuring forces and moments with application to ground vehicle design and engineering”, Proceedings ASME IMECE 2005.
6. Gobbi M., Previati G., Mastinu G., “Refinement design of a measuring wheel”, Proceedings ASME DETC2011, August 2011, Washington, DC, USA.
7. APOLLO: Intelligent tire for Accident-free Traffic, Project no. IST-2001-34372, 2002
8. Bicchi A., “A criterion for optimal design of Multiaxis Force Sensors”, Journal of Robotics and Autonomous Systems, 10 (4), 1992.
9. http://www.michsci.com/ Michigan Scientific Corporation (model LW 12.8), 10/2014.
10. http://www.mts.com/ MTS Systems Corporation (SWIFT Wheel Force Transducer), 10/2014.
11. http://www.ati-ia.com/ATI Industrial Automation, (Series OMEGA and GAMMA), 10/2014.
12. http://www.kistler.com/ Kistler (RoaDyn Wheel Force Sensor), 10/2014.
13. http://www.michsci.com/Products/transducers/SpecificationsLW-MC3.5KWheelLoadTransducerMichiganScientificCorporation-.htm(Motorcycle Wheel Force Transducer Specifications), 12/2014.
14. Mastinu G., Gobbi M., “Device and method for measuring forces and moments”, US Patent 7665371 B2, 23/02/2010.
15. Mastinu G., Gobbi M., “Dispositivo e metodo per la misura di forze e momenti”, Italian Patent MI2003A 001500, 22/07/2003.
16. Mastinu G., Gobbi M., Previati G., A new six-axis load cell. Part I: Design, Exp. Mech. 51 (3) (2011) 373-388, doi:10.1007/s11340-010-9355-1.
17. Gobbi M., Previati G., Guarneri P., Mastinu G., A new six-axis load cell. Part II: error analysis, construction and experimental assessment of performances, Exp. Mech. 51 (3) (2011) 389-399, DOI:10.1007/s11340-010-9350-6.
18. Mastinu G., Gobbi M., “Giunto elastico a cerniera sferica traslante e sensore di forze e momenti perfezionato con tale giunto”, Italian Patent, ME.05.025.A, 22/05/2006.
19. Mastinu G., Gobbi M., “Elastic joint with translating spherical hinge and force and moment sensor improved by means of the said joint”, US Patent US7779705 B2, Aug 24, 2010
20. Gobbi M. “A k, k-ε optimality selection based multi objective genetic algorithm with applications to vehicle engineering”, Optimization and Engineering, June 2013, Volume 14, Issue 2, pp 345-360.
21. Young W.C., Budynas R.G., Roark's formulas for stress and strain, seventh ed., McGraw-Hill, 2001.
22. Mastinu G, Gobbi M, Miano C (2006). Optimal Design of Complex Mechanical Systems With Applications to Vehicle Engineering. ISBN: 3-540-34354-7. BERLIN: Springer Verlag.
23. Suresh S., “Fatigue of Materials (Cambridge Solid State Science Series) Second Edition”, Chapter 7, Cambridge University Press, 1998.
24. Sines, G., Waisman, J.L., “Metal Fatigue”, McGraw-Hill Inc. New York, 1959.
25. Gobbi M., Mastinu G., Previati G., Pennati M., “6-Axis Measuring Wheels for Trucks or Heavy Vehicles”, SAE International Journal of Commercial Vehicles, Volume 7, Issue 1, May 2014, Pages 141-149.
26. Ballo, F., Gobbi M., Mastinu G., Previati G., “Advances in Force and Moments Measurements by an Innovative Six-axis Load Cell”, Experimental Mechanics, April 2014, Volume 54, Issue 4, pp 571-592.
27. Gobbi, M., Haque, I., Papalambros, P. Y., and Mastinu, G., “Optimization and integration of ground vehicle systems”, Vehicle System Dynamics, Vol. 43, No. 6-7, 2005, 437-453.